Sensors and Materials, Vol. 32, No. 4 (2020) 1357–1364
MYU Tokyo

S & M 2181

Scintillation Characteristics of Pr-doped $Gd_2Si_2O_7$ Single Crystal

Prom Kantuptim,* Masaki Akatsuka, Daisuke Nakauchi,
Takumi Kato, Noriaki Kawaguchi, and Takayuki Yanagida

Division of Materials Science, Graduate School of Science and Technology,
Nara Institute of Science and Technology, 8916-5 Takayama, Ikoma, Nara 630-0192, Japan

(Received December 3, 2019; accepted March 2, 2020)

Keywords: gadolinium pyrosilicate, decay time, floating zone method, Pr^{3+}, photoluminescence

Pr-doped gadolinium pyrosilicate, which had a composition of $Gd_2Si_2O_7$, was synthesized by the floating zone method with different Pr concentrations from 0.1 to 2.0 mol%. After confirming the crystal phase by X-ray diffraction analysis, photoluminescence (PL) and scintillation properties were investigated. PL emission spectra showed a broad emission peak at 340–360 nm due to Pr^{3+} 5d–4f transition, and decay times were around 9–12 ns. In X-ray-induced scintillation spectra, we confirmed a similar spectral shape with PL, and scintillation decay times were around 18–29 ns. In the ^{137}Cs γ-ray-irradiated pulse height measurement, the 1.0% Pr-doped sample had shown the highest scintillation light yield of 2290 ph/MeV among the present samples. In the same setup, we also used different γ-ray sources to check the energy response linearity. Finally, energy resolution as a function of γ-ray energy was investigated.

1. Introduction

Scintillators are materials that have an ability to convert charged particles, neutrons or high-energy photons, such as X- and γ-rays, into low-energy electromagnetic waves such as ultraviolet, visible, and infrared light.[1–4] In the present day, scintillators have been used as radiation detectors by combining with a photodetector, and a radiation sensor consisting of a scintillator and a photodetector has been called a scintillation detector. Moreover, scintillation detectors have been used in many scientific areas, such as X-ray scanners for a security system,[5] environmental radiation monitoring,[6] positron emission tomography in medical diagnosis,[7] natural resource exploration,[8] and a specific sensor for high-energy physics research.[9] The selection of materials for solid-state scintillators is very wide, from single crystals,[10] transparent ceramics,[11] organics,[12] and hybrid compounds[13] to glass.[14] Although we have a wide freedom to select materials, candidate materials must have a large volume (bulk form) and a high transparency.[15] Bulk materials are preferable for maximizing the interaction probability between ionizing radiation and a scintillator. At the same time,

*Corresponding author: e-mail: prom.kantuptim.pf2@ms.naist.jp
https://doi.org/10.18494/SAM.2020.2726

ISSN 0914-4935
https://myukk.org/

transparent materials are ideal because generated photons must be delivered to photodetectors while minimizing self-absorption. In addition, the development of a novel scintillator also requires three more properties, which are high scintillation light yield, high energy resolution, and short scintillation decay time.[16]

In X- and γ-ray scintillation detectors, the single crystal with a high effective atomic number (Z_{eff}) activated with a rare-earth ion as the luminescence center has received much attention.[17] Among rare-earth ions, Pr^{3+} becomes a potential candidate for a luminescence center owing to its short scintillation decay time of around 20 ns when doped in the LuAG host.[18] In addition, Pr^{3+} can exhibit $5d^14f^1$–$4f^2$ ($^3H_4$, $^3H_5$, $^3H_6$, $^3F_{3(4)}$) transition,[19,20] which shows a relatively faster scintillation decay than other rare-earth ions, such as Ce^{3+}, in similar host materials.[21–23] For host materials, materials in the pyrosilicate group, such as $Gd_2Si_2O_7$ (GPS), $Lu_2Si_2O_7$ (LPS), and $Y_2Si_2O_7$ (YPS), have become more attractive[24–26] owing to their high Z_{eff}, chemical-thermal stability, and preferable scintillation characteristics under γ-ray irradiation.[27]

Recently, a comparative study of LPS, YPS, and GPS single crystals doped with Pr and undoped $Pr_2Si_2O_7$ (PrPS) has successfully been performed at a fixed Pr doping concentration of 1.0 mol%.[28] Despite recent advancements, it is necessary to investigate more the Pr concentration dependence of the GPS crystal. In this work, GPS single crystals with different Pr doping concentrations were systematically studied in terms of both photoluminescence (PL) and scintillation properties, such as PL emission spectrum, PL decay time, scintillation spectrum, scintillation decay time, scintillation light yield, and energy resolution.

2. Materials and Methods

Five samples were prepared with different Pr concentrations of 0.1, 0.3, 0.5, 1.0, and 2.0 mol% with respect to Gd. First, the mixed powder was prepared by using high-purity powders of Gd_2O_3 (99.99%), SiO_2 (99.999%), and Pr_6O_{11} (99.99%). After mixing these powders, hydrostatic pressure was applied for shaping samples into cylinder rods. Then, we sintered the rod samples in an electric furnace at 1200 °C for 8 h under air atmosphere. After obtaining solid ceramic rods, each sample was crystallized by using a floating zone (FZ) furnace (Canon Machinery FZD0192) with a growth rate of 5 mm/h and the heat generated by two halogen lamps. After the crystal growth, each sample was cut to a suitable size for further measurements. Powder X-ray diffraction (XRD) analysis was conducted to investigate the phase of the samples using MiniFlex600 (Rigaku). The X-ray source is a conventional X-ray tube with a Cu Kα target operated at 40 kV and 15 mA and in the 2θ range of 10–40°.

As a PL property, PL emission spectra were evaluated by Quantaurus-τ (Hamamatsu Photonics C11367) and observed at an excitation wavelength of 280 nm and an emission wavelength from 300 to 500 nm with a 300 nm shotcut filter (Asahi spectra, SCF300). Based on the emission and excitation wavelengths, PL decay time profiles were also evaluated by the same instrument as PL spectra. To observe emission from Pr^{3+} 5d–4f transition, a 280 nm LED was used as the excitation source, and the observation wavelength was 350 nm.

Scintillation properties, such as scintillation spectra, scintillation decay time, and pulse height (PH) spectra, were investigated. The scintillation spectrum was evaluated using our

original setup.[29] X-ray-induced scintillation decay time profiles were also measured using our original setup.[30] The pulsed X-ray tube with a tungsten anode was used as an X-ray source in this measurement and operated at a voltage of 30 kV. Scintillation was detected using a photomultiplier tube (PMT) (Hamamatsu R7207-01), and the wavelength sensitivity ranged from 160 to 650 nm.

To investigate γ-ray-induced scintillation detector properties, PH measurements were conducted using our original setup.[31] Each sample was attached to the PMT (Hamamatsu R7600-200) using optical grease (OKEN 6262A). ^{137}Cs (662 keV) was selected as the γ-ray source to evaluate the light yield. The photons emitted from the sample were collected using the PMT. Then, the signals from the PMT were fed to a preamplifier (ORTEC 113), a shaping amplifier (ORTEC 572) with 2 μs shaping time and a multichannel analyzer (MCA) (Amptek Pocket MCA). Finally, the signals were sent to a personal computer. In the PH analysis, the scintillation light yield was calibrated using 1.0 mol% Pr-doped LPS, which had a light yield of 9700 ph/MeV[28] with a similar emission spectrum to that of Pr-doped GPS. The linearity and energy resolution were evaluated using the same setting to that of various γ-ray sources such as ^{22}Na (511 keV), ^{57}Co (122 keV), ^{133}Ba (356 keV), ^{137}Cs (662 keV), and ^{241}Am (60 keV). All measurements in this study were performed at room temperature.

3. Results and Discussion

3.1 Sample synthesis

The single-crystal rods obtained from the FZ method were 20–30 mm in length and 4 mm ϕ with a notable crack along the rod length. Figure 1 shows a photograph of the as-grown single-crystal rod and cut and polished sample pieces for the measurement. The samples appeared colorless to light yellow depending on the Pr concentration. Figure 2 presents the powder XRD patterns of all the samples including the undoped GPS for reference (COD 9011106). All the samples had a diffraction pattern similar to the reference, and no impurity phase from the Gd_2O_3–SiO_2 phase diagram[32] was detected.

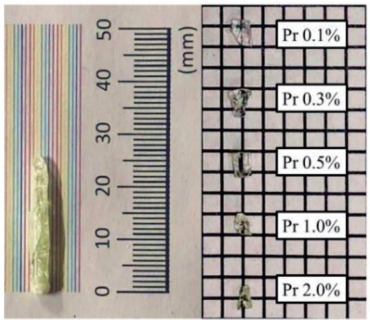

Fig. 1. (Color online) Pr:GPS single crystals of (left) as-grown and (right) cut pieces.

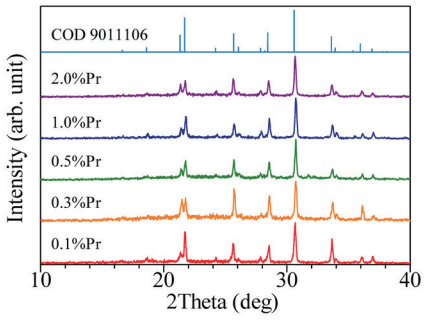

Fig. 2. (Color online) Powder XRD patterns of GPS doped with different Pr concentrations.

3.2 PL properties

Figure 3 presents PL emission spectra of all the Pr:GPS samples observed upon 280 nm excitation. Two emission peaks were observed. The intense emission peak from 310 nm resulted in the Gd^{3+} 4f–4f transition from the host's triclinic GPS phase. The broad emission around 340–360 originated from the 5d–4f transition of Pr^{3+}.[33] In the 0.1 and 0.3% Pr-doped samples, we observed only a clear emission from Gd^{3+}. On the other hand, the emission from Pr^{3+} became more intense in the 0.5 and 1.0% Pr-doped samples. In the 2.0% Pr-doped sample, we observed that both emission peaks merged around 330 nm. The relationship can be understood from the excitation energy ratio delivered to Gd^{3+} and Pr^{3+}. In the PL decay time study, we took the 350 nm emission for the monitoring wavelength of the 5d–4f transition of Pr^{3+}. PL decay time profiles are shown in Fig. 4. To deduce decay times, decay curves were approximated by the sum of two exponential functions. Table 1 presents the PL decay time. We observed a Pr^{3+} 5d–4f characteristic decay time of around 9–12 ns in all the samples, represented as the 2nd exponential decay time. In addition, the 1st exponential decay time of around 2 ns appearing in all the samples originated from the instrumental response function (IRF). If we deconvolute the IRF ideally, the 1st component is not detected. However, from our experience, perfect deconvolution is difficult and such a fast component is often detected. In Pr-doped GPS, such a fast component is physically impossible, and we assign the origin of the 1st component as the IRF.

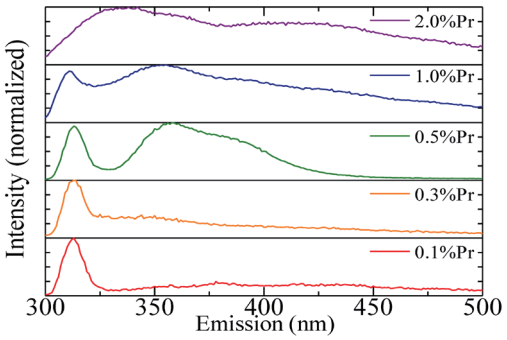

Fig. 3. (Color online) PL emission spectra observed at excitation wavelength of 280 nm.

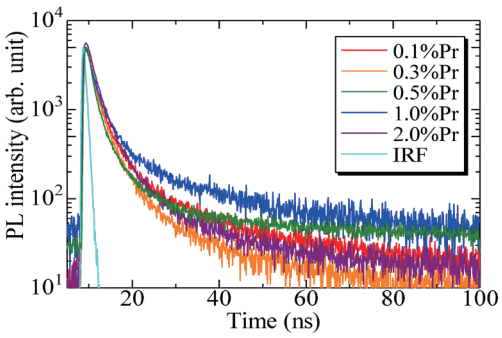

Fig. 4. (Color online) PL decay time profiles upon 280 nm excitation monitoring at 350 nm.

Table 1
PL and scintillation decay times of Pr:GPS samples.

Sample	PL decay time (ns)		Scintillation decay time (ns)	
	1st exp	2nd exp	1st exp	2nd exp
Pr 0.1% GPS	1.89	10.67	0.64	22.43
Pr 0.3% GPS	1.81	8.85	0.65	18.48
Pr 0.5% GPS	1.52	10.57	0.67	17.94
Pr 1.0% GPS	1.86	11.69	0.66	29.93
Pr 2.0% GPS	2.06	9.94	0.64	24.51

3.3 Scintillation properties

Figure 5 presents the X-ray-induced scintillation spectra of Pr:GPS samples. The spectral shapes were similar in all the samples. This measurement did not represent the quantitative value of the scintillation intensity but only the qualitative value, and we could not compare the emission intensities of our samples. The sharp and intense emission line observed at 310 nm and a small peak at 320 nm originated from the Gd^{3+} 4f–4f transition. The broad emission from 340 to 410 nm originated from the 5d–4f transition of Pr^{3+}.[28,34] The scintillation decay time profiles are shown in Fig. 6. The decay curves were approximated by the sum of two exponential functions. Table 1 also presents the scintillation decay times. Analogous to the PL decay time, the 2nd component originated from the Pr^{3+} 5d–4f transitions with values of 18–29 ns. Besides, the 1st exponential decay time of around 0.6 ns appeared in all the samples originated from the IRF. The longer decay times observed in the 1.0 and 2.0 mol% Pr-doped samples would be caused by the delayed recombination.[35]

Figure 7 presents the PH spectra of Pr:GPS samples under γ-ray irradiation from ^{137}Cs. Photoabsorption peaks of the 0.1, 0.3, 0.5, 1.0, and 2.0% Pr-doped samples were observed at 180, 200, 210, 770, and 520 channels, respectively. Taking into account the light yield with the reference sample of 1.0% Pr-doped LPS,[28] the absolute scintillation light yields of 0.1, 0.3, 0.5, 1.0, and 2.0% Pr-doped samples were 530, 600, 640, 2290, and 1550 ph/MeV, respectively. In this measurement, the typical error for the light yield was ±10%. The relationship between scintillation light yield and Pr concentration is presented in Fig. 8. As a result, the optimum Pr concentration in GPS for scintillation light yield is around 1.0%. The function shape between dopant concentration and scintillation light yield can be understood from the balance of the increase in the number of emission centers and the self-absorption effect. Such an empirical model well fits the results of Ce-doped YAG, and the detailed explanation can be found elsewhere.[36]

Figure 9 demonstrates the relationship between the number of photoabsorption peak channels and γ-ray energy, namely, energy response linearity. In this analysis, we selected 1.0 and 2.0%

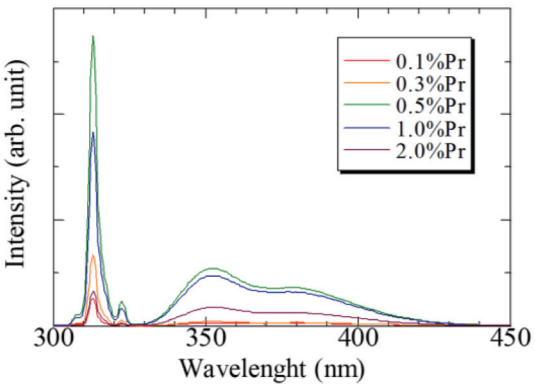

Fig. 5. (Color online) X-ray-induced scintillation spectra of Pr:GPS samples.

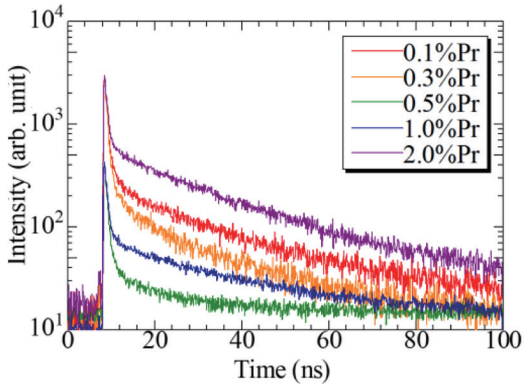

Fig. 6. (Color online) X-ray-induced scintillation decay time profiles of Pr:GPS samples.

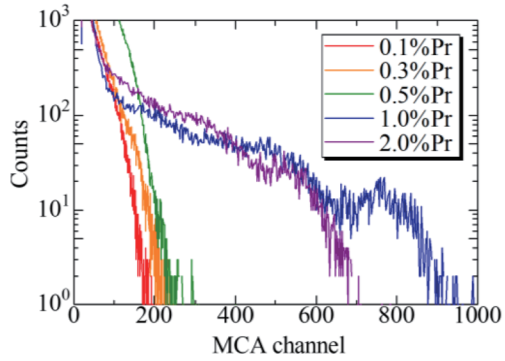

Fig. 7. (Color online) ^{137}Cs γ-ray-irradiated PH spectra of Pr:GPS samples.

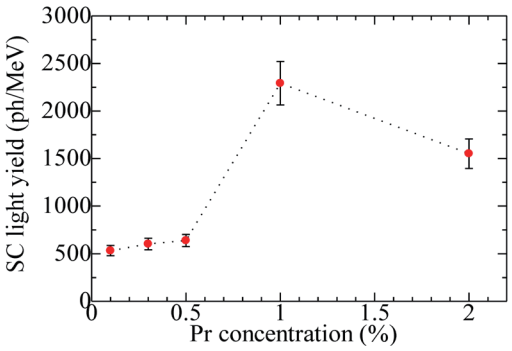

Fig. 8. (Color online) ^{137}Cs γ-ray-irradiated scintillation light yield as a function of Pr concentration in Pr:GPS samples.

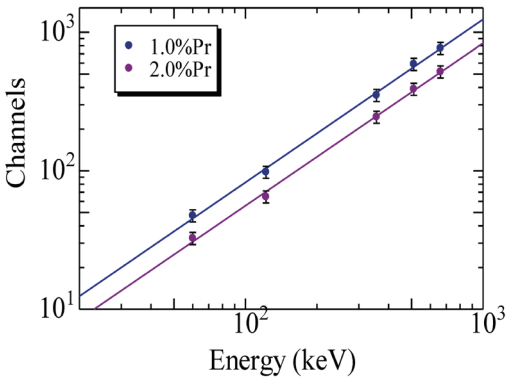

Fig. 9. (Color online) Relationship between γ-ray energy and scintillation light yield of the Pr:GPS samples.

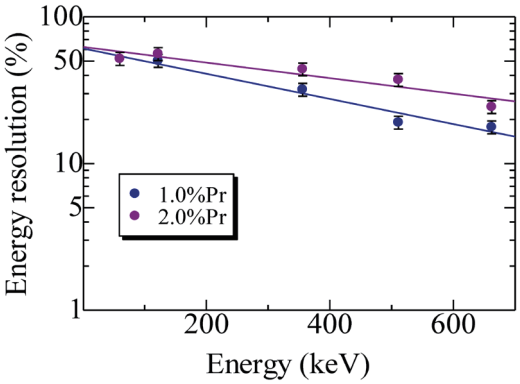

Fig. 10. (Color online) Energy resolutions of Pr:GPS samples as a function of γ-ray enegy.

Pr-doped samples since the other samples did not show clear photoabsorption peaks. The 1.0 and 2.0% Pr-doped samples had a quite linear response against γ-ray energy. On the other hand, Fig. 10 shows the energy resolutions of the 1.0 and 2.0% Pr-doped samples as a function of γ-ray energy. The monotonic decrease in energy resolution proportional to γ-ray energy was observed. Thus, the number of photon statistics was dominant in the energy resolution in the present samples. At 662 keV from ^{137}Cs irradiation, the energy resolution was determined to be 17.7 and 24.4% for the 1.0 and 2.0% Pr-doped samples, respectively.

4. Conclusions

GPS single crystals doped with 0.1, 0.3, 0.5, 1.0, and 2.0% Pr were successfully synthesized by the FZ method. All of the samples had a single phase without any impurity phases according to powder XRD patterns. In PL properties, we found the emission of Pr^{3+} 5d–4f transition with a PL decay time of 9–12 ns. X-ray-induced scintillation emission spectra were evaluated in all

the samples with characteristic scintillation decay times of around 19–30 ns. In ^{137}Cs-irradiated PH measurement, the scintillation light yield of Pr:GPS reached up to 2290 ph/MeV in the 1% Pr-doped sample. Under γ-ray irradiations of different energies from radioisotopes, a monotonical decrease in energy resolution was observed. Throughout this study, we conclude that the optimum Pr concentration in GPS in the scintillation properties is ~1 mol%.

Acknowledgments

This work was supported by Grants-in-Aid for Scientific Research A (17H01375) and B (18H03468 and 19H03533), Young Scientists B (17K14911), and Early-Career Scientists (18K14158) from JSPS. The Cooperative Research Project of Research Institute of Electronics, Shizuoka University, Murata Foundation, and Nippon Sheet Glass Foundation are also acknowledged.

References

1 T. Yanagida: Proc. Japan Academy, Ser. B, Physical and Biological Sciences **94** (2018) 75.
2 C. W. E. Van Eijk: Nucl. Instrum. Methods Phys. Res., Sect. A **460** (2001) 1.
3 P. Dorenbos: Phys. Status Solidi Appl. Mater. Sci. **202** (2005) 195.
4 W. W. Moses: Nucl. Instrum. Methods Phys. Res., Sect. A **487** (2002) 123.
5 J. Glodo, Y. Wang, R. Shawgo, C. Brecher, R. H. Hawrami, J. Tower, and K. S. Shah: Phys. Procedia **90** (2017) 285.
6 K. Watanabe, T. Yanagida, K. Fukuda, A. Koike, T. Aoki, and A. Uritani: Sens. Mater. **27** (2015) 269.
7 C. L. Melcher: J. Nucl. Med. **41** (2000) 1051.
8 T. Yanagida, Y. Fujimoto, S. Kurosawa, K. Kamada, H. Takahashi, Y. Fukazawa, M. Nikl, and V. Chani: Jpn. J. Appl. Phys. **52** (2013) 3.
9 H. Takahashi, T. Yanagida, D. Kasama, T. Ito, M. Kokubun, K. Makishima, T. Yanagitani, H. Yagi, T. Shigeta, and T. Ito: IEEE Trans. Nucl. Sci. **53** (2006) 2404.
10 D. Nakauchi, N. Kawaguchi, and T. Yanagida: Sens. Mater. **31** (2019) 1249.
11 H. Kimura, T. Kato, D. Nakauchi, M. Koshimizu, N. Kawaguchi, and T. Yanagida: Sens. Mater. **31** (2019) 1265.
12 T. Yanagida, K. Watanabe, and Y. Fujimoto: Nucl. Instrum. Methods Phys. Res., Sect. A **784** (2015) 111.
13 N. Kawano, M. Koshimizu, G. Okada, Y. Fujimoto, N. Kawaguchi, T. Yanagida, and K. Asai: Sci. Rep. **7** (2017) 14754.
14 N. Kawaguchi and T. Yanagida: Sens. Mater. **31** (2019) 1257.
15 M. Moszynski: Nucl. Instrum. Methods Phys. Res., Sect. A **505** (2003) 101.
16 W. Setyawan, R. M. Gaume, R. S. Feigelson, and S. Curtarolo: IEEE Trans. Nucl. Sci. **56** (2009) 2989.
17 T. Yanagida: Opt. Mater. (Amst). **35** (2013) 1987.
18 T. Yanagida: J. Lumin. **169** (2016) 544.
19 V. Gorbenko, Y. Zorenko, V. Savchyn, T. Zorenko, A. Pedan, and V. Shkliarskyi: Radiat. Meas. **45** (2010) 461.
20 N. Kawaguchi, H. Kimura, M. Akatsuka, G. Okada, N. Kawano, K. Fukuda, and T. Yanagida: Sens. Mater. **30** (2018) 1585.
21 D. Nakauchi, Y. Yoshida, N. Kawaguchi, and T. Yanagida: J. Mater. Sci. Mater. Electron. **30** (2019) 14085.
22 D. Nakauchi, G. Okada, N. Kawano, N. Kawaguchi, and T. Yanagida: Appl. Phys. Express **10** (2017) 072601.
23 D. Nakauchi, G. Okada, N. Kawano, N. Kawaguchi, and T. Yanagida: Jpn. J. Appl. Phys. **57** (2018) 2.
24 I. Gerasymov, O. Sidletskiy, S. Neicheva, B. Grinyov, V. Baumer, E. Galenin, and K. Katrunov: J. Cryst. Growth **318** (2011) 805.
25 P. Dorenbos, M. Marsman, C. W. E. Van Eijk, M. V. Korzhik, and B. I. Minkov: Radiat. Eff. Defects Solids **135** (1995) 325.
26 L. Pidol, O. Guillot-Noël, A. Kahn-Harari, B. Viana, D. Pelenc, and D. Gourier: J. Phys. Chem. Solids **67** (2006) 643.
27 L. Pidol, A. Khan-Harari, B. Viana, B. Ferrand, P. Dorenbos, J. T. M. De Haas, C. W. E. Van Eijk, and E. Virey: J. Phys. Condens. Matter **15** (2003) 2091.

28 T. Yanagida, K. Watanabe, G. Okada, and N. Kawaguchi: Jpn. J. Appl. Phys. **57** (2018) 106401.
29 T. Yanagida, K. Kamada, Y. Fujimoto, H. Yagi, and T. Yanagitani: Opt. Mater. (Amst). **35** (2013) 2480.
30 T. Yanagida, Y. Fujimoto, T. Ito, K. Uchiyama, and K. Mori: Appl. Phys. Express **7** (2014) 18.
31 T. Yanagida, N. Kawaguchi, Y. Fujimoto, K. Fukuda, K. Watanabe, A. Yamazaki, and A. Uritani: J. Lumin. **144** (2013) 212.
32 V. Baumer, I. Gerasymov, O. Sidletskiy, O. Voloshina, and S. Neicheva: J. Alloys Compd. **509** (2011) 8478.
33 Y. Tsubota, J. H. Kaneko, M. Higuchi, S. Kawamura, S. Nishiyama, F. Fujita, S. Ueda, K. Kurashige, H. Ishibashi, A. Homma, and M. Furusaka: Prog. Nucl. Sci. Technol. **1** (2011) 288.
34 W. Drozdowski, T. Lukasiewicz, A. J. Wojtowicz, D. Wisniewski, and J. Kisielewski: J. Cryst. Growth **275** (2005) e709.
35 V. B. Mikhailik, Y. Elyashevskyi, H. Kraus, H. J. Kim, V. Kapustianyk, and M. Panasyuk: Nucl. Instrum. Methods Phys. Res., Sect. A **792** (2015) 1.
36 T. Yanagida, H. Takahashi, T. Ito, D. Kasama, T. Enoto, M. Sato, S. Hirakuri, M. Kokubun, K. Makishima, T. Yanagitani, H. Yagi, T. Shigeta, and T. Ito: IEEE Trans. Nucl. Sci. **52** (2005) 1836.